



SPARC-FEL-12/001
Revised March 20, 2012

Focusing properties of SPARC undulator

M. Quattromini, M. Artioli, E. Di Palma, L. Giannessi and A. Petralia
C.R.E. ENEA-Frascati, Via E. Fermi 45, 00044 Frascati (Rome) Italy

In this note the focusing properties of magnetic undulators are addressed, with particular emphasis to SPARC-type undulators, i.e. linear devices weakly defocusing in the horizontal (wiggling) plane and strongly focusing in the vertical plane. The beam trajectory will be derived in detail to different approximation levels. Some subtleties will be discussed aiming at obtaining a matrix expression suitable for customary beam optics and matching. The purpose of this note is to clarify the theoretical framework necessary for the deployment of a numerical code added to SPARC Control System as a tool to be used at runtime. In particular, a considerable analytical effort has been devoted to the problem of identifying the conditions that ensure the existence of the electron beam eigenstates in the undulator lattice for a given working set of e-beam energy and resonant wavelength.

I. INDUCTION FIELD FOR PURE PERMANENT MAGNET LINEAR UNDULATORS.

It can be shown that magnetic field for a pure permanent magnet undulator can be derived from a magnetostatic potential:

$$\vec{B} = -\vec{\nabla}\Phi_M \quad (1)$$

Eq. (1) follows from the fact that, in absence of currents ($\vec{J} = 0$), the Ampère law reads:

$$\vec{\nabla} \times \vec{B} = 0 \quad (2)$$

Proceeding in a fairly axiomatic fashion (literature abounds of textbooks and monographs where this topic is discussed in detail), for the magnetic potential Φ_M the following expression will be considered:

$$\Phi_M = -\frac{B_0}{k_y} \cos(k_x x) \sinh(k_y y) \sin(k_u z) \quad (3)$$

Magneto-static potential (3) is only one of several possible forms that give rise to a magnetic field which is *i*) periodic (sinusoidal) in the longitudinal (z) direction; *ii*) mainly oriented along one of the two transverse directions (y) and *iii*) essentially decoupled along the other (x). The form (3) implicitly reflects some peculiar properties of SPARC undulators, namely that of being slightly defocusing in the horizontal (wiggling) plane, and strongly focusing in the vertical (main field) direction. Other expressions are possible, reflecting different focusing properties of undulators (e.g. undulators focusing in both directions, or with different polarizations). Eq. (1) implies the following expressions of field's components:

$$\begin{aligned} B_x(x, y, z) &= -\frac{k_x}{k_y} B_0 \sin(k_x x) \sinh(k_y y) \sin(k_u z) \\ B_y(x, y, z) &= B_0 \cos(k_x x) \cosh(k_y y) \sin(k_u z) \\ B_z(x, y, z) &= \frac{k_u}{k_y} B_0 \cos(k_x x) \sinh(k_y y) \cos(k_u z) \end{aligned} \quad (4)$$

The condition of magnetic field to be solenoidal

$$\vec{\nabla} \cdot \vec{B} = \nabla^2 \Phi_M = 0$$

translates for (4) to:

$$k_y^2 - k_x^2 = k_u^2$$

On axis ($x, y \approx 0$)

$$B_x(x, y, z) \approx -B_0 k_x^2 x y \sin(k_u z)$$

$$B_y(x, y, z) \approx B_0 \left(1 - \frac{k_x^2 x^2}{2}\right) \left(1 + \frac{k_y^2 y^2}{2}\right) \sin(k_u z)$$

$$B_z(x, y, z) \approx B_0 k_u y \left(1 - \frac{k_x^2 x^2}{2}\right) \cos(k_u z)$$

To second order field components reduce to

$$B_x(x, y, z) \approx -B_0 k_x^2 x y \sin(k_u z)$$

$$B_y(x, y, z) \approx B_0 \left(1 - \frac{k_x^2 x^2}{2} + \frac{k_y^2 y^2}{2}\right) \sin(k_u z)$$

$$B_z(x, y, z) \approx B_0 k_u y \cos(k_u z)$$

which can be further manipulated to read

$$B_x(x, y, z) \approx -B_0 \delta \frac{k_u^2}{2} x y \sin(k_u z)$$

$$B_y(x, y, z) \approx B_0 \left\{1 + \frac{k_u^2}{4} [-\delta x^2 + (2 + \delta) y^2]\right\} \sin(k_u z) \quad (5)$$

$$B_z(x, y, z) \approx B_0 k_u y \cos(k_u z)$$

where

$$\delta = 2 \frac{k_x^2}{k_u^2} \quad (6)$$

The value of δ defined in eq. (6) has been calculated as a function of the gap for an idealized SPARC undulator section (fig. (1)) modeled with RADIA[1–3]. The results are shown in fig. (1) along with a fit to a straight line:

$$\delta(g) = a + b \cdot g \quad a \approx -9.11 \cdot 10^{-3} \quad b \approx 1.18 \cdot 10^{-3} \text{ mm}^{-1} \quad (7)$$

II. TRAJECTORY OF A RELATIVISTIC ELECTRON IN A PPM UNDULATOR

In this section some basic results will be re-derived[4] about the dynamics of an electron beam in the field of a magnetic undulator. A reference frame oriented as shown in fig. (1) will be used throughout this report, so that the the main component of the field is directed along the y axis, while electron beam propagates along the $+z$ axis. In first instance, the motion in the horizontal (that is, $x - z$) plane will be discussed, all field's components will be neglected but B_y and $B_y = B_0 \sin(k_u z)$ will be assumed. It follows that:

$$\frac{d\vec{p}}{dt} = \gamma m c \frac{d\vec{\beta}}{dt} = e \vec{v} \times \vec{B} = e c \vec{\beta} \times \vec{B} = -e c B_y (\beta_z \hat{u}_x - \beta_x \hat{u}_z)$$

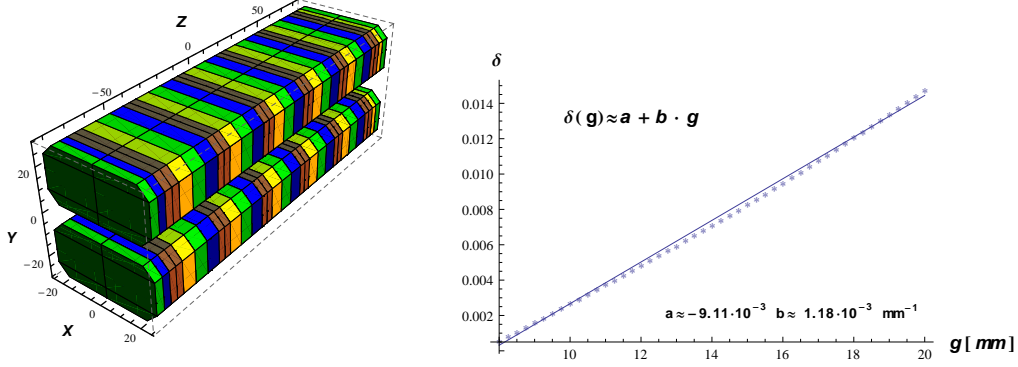


Figure 1

The RADIA model of SPARC undulator. Right: parameter δ as defined in (6) as a function of the gap.

where e is the electron's charge and it has been implicitly assumed that the particle energy is left unchanged ($\dot{\gamma} = 0$) by the interaction with a pure magnetic field. The transverse force acting upon an electron is then purely horizontal and given by

$$\frac{d\beta_x}{dt} \approx -\frac{e}{\gamma m} B_y \beta_z$$

Since $\beta_x \ll \beta_z \approx 1$ one can assume no longitudinal acceleration:

$$\frac{d\beta_z}{dt} \approx \frac{e}{\gamma m} \beta_x B_y \approx 0$$

so that

$$\beta_z c dt \approx dz \quad (8)$$

and

$$\frac{d\beta_x}{dz} \approx -\frac{e}{\gamma m c} B_y \quad (9)$$

Note that

$$\beta_x = \frac{1}{c} \frac{dx}{dt} = \beta_z \frac{dx}{dz}$$

implying that

$$\frac{d^2 x}{dz^2} \approx -\frac{e}{\gamma \beta_z m c} B_y \quad (10)$$

Direct integration yields

$$\frac{dx}{dz} \equiv x'(z) = x'(0) - \frac{e}{\gamma \beta_z m c} \int_0^z B_y(\zeta) d\zeta \quad (11)$$

A further integration yields:

$$x(z) = x(0) + x'(0)z - \frac{e}{\gamma \beta_z m c} \int_0^z \int_0^{\zeta_2} B_y(\zeta_1) d\zeta_1 d\zeta_2 \quad (12)$$

Since $B_y(\zeta) = B_0 \sin(k_u \zeta)$ then

$$\begin{aligned} \int_0^z \int_0^{\zeta_2} B_y(\zeta_1) d\zeta_1 d\zeta_2 &= \int_0^z B_0 \frac{1 - \cos(k_u \zeta)}{k_u} d\zeta_2 \\ &= B_0 \frac{k_u z - \sin(k_u z)}{k_u^2} \end{aligned}$$

and the expression of horizontal vs longitudinal position reads

$$x(z) = x(0) + x'(0)z - \frac{e}{\gamma\beta_z mc} B_0 \frac{k_u z - \sin(k_u z)}{k_u^2} \quad (13)$$

The requirement that the trajectory wiggles around the entrance position, i.e.

$$x(\lambda_u) = x(0) \quad (14)$$

implies (observe that $k_u \lambda_u = 2\pi$)

$$x'(0)\lambda_u - \frac{eB_0}{\gamma\beta_z mc} \frac{2\pi}{k_u^2} = 0$$

that is

$$x'(0) = \frac{eB_0}{\gamma\beta_z mc k_u} = \frac{1}{\gamma\beta_z} \frac{eB_0 \lambda_u}{2\pi mc}$$

Since the K (peak) parameter for a linear undulator is by definition

$$K = -\frac{eB_0 \lambda_u}{2\pi mc} \quad (15)$$

(note that electron charge is negative) it follows

$$x'(0) = -\frac{K}{\gamma\beta_z} \approx -\frac{K}{\gamma}$$

The reference trajectory is then

$$\begin{aligned} x(z) &= x(0) + \frac{e}{\gamma\beta_z mc} B_0 \frac{\sin(k_u z)}{k_u^2} \\ &= x(0) + \frac{eB_0 \lambda_u}{2\pi\gamma\beta_z mc} \frac{\sin(k_u z)}{k_u} \\ &= x(0) - \frac{K}{\gamma\beta_z} \frac{\sin(k_u z)}{k_u} \approx x(0) - \frac{K}{\gamma} \frac{\sin(k_u z)}{k_u} \end{aligned} \quad (16)$$

Eq. (16) defines the horizontal reference trajectory for a particle entering the undulator on axis ($x(0) = 0$), neglecting off axis corrections in field expression (4) or (5):

$$x_r(z) = -\frac{K}{\gamma} \frac{\sin(k_u z)}{k_u} = -\frac{\lambda_u}{2\pi} \frac{K}{\gamma} \sin(k_u z) \quad (17)$$

The trajectory of an electron traveling off the reference orbit by an amount $x_\delta(z)$ reads obviously

$$x(z) = x_r(z) + x_\delta(z) \quad (18)$$

Horizontal acceleration (10) can be modified by introducing corrected field B_y according to (5) (with $y = 0$)

$$\frac{d^2 x}{dz^2} = \frac{d^2 x_r}{dz^2} + \frac{d^2 x_\delta}{dz^2} = -\frac{e}{\gamma\beta_z mc} B_y^0(z) \left\{ 1 - \frac{k_u^2}{4} \delta [x_r(z) + x_\delta(z)]^2 \right\} \quad (19)$$

where $B_y^0(z) \equiv B_y(x = y = 0, z)$. On the other hand

$$\frac{d^2 x_r}{dz^2} = -\frac{e}{\gamma\beta_z mc} B_y(z) = -\frac{e}{\gamma\beta_z mc} B_y^0(z) \left[1 - \frac{k_u^2}{4} \delta x_r^2(z) \right]$$

The approximation

$$[x_r(z) + x_\delta(z)]^2 \approx x_r^2(z) + 2x_r(z)x_\delta(z)$$

yields finally

$$\begin{aligned}
\frac{d^2 x_\delta}{dz^2} &= \frac{e}{\gamma \beta_z m c} B_y^0(z) \frac{k_u^2}{2} \delta x_r(z) x_\delta(z) \\
&= -\frac{1}{\gamma^2 \beta_z} \frac{e B_0 \lambda_u}{2 \pi m c} \sin^2(k_u z) \frac{k_u^2}{2} \delta K x_\delta(z) \\
&= \frac{\delta}{2 \gamma^2 \beta_z} K^2 k_u^2 \sin^2(k_u z) x_\delta(z) \\
&\approx \frac{\delta}{2 \gamma^2} K^2 k_u^2 \sin^2(k_u z) x_\delta(z)
\end{aligned} \tag{20}$$

(where for $x_r(z)$ the approximation (17) has been used). Averaging over a period the $\sin^2(k_u z)$ term yields a factor 1/2:

$$\left\langle \frac{d^2 x_\delta}{dz^2} \right\rangle \approx \frac{\delta}{4 \gamma^2} K^2 k_u^2 x_\delta(z)$$

that is

$$\boxed{\left\langle \frac{d^2 x_\delta}{dz^2} \right\rangle \approx \delta \left(\frac{\pi K}{\gamma \lambda_u} \right)^2 x_\delta(z)} \tag{21}$$

A similar calculation can be performed to obtain the governing equation for y . Observe first that

$$\frac{d\beta_y}{dt} \approx \frac{e}{\gamma m} (\beta_z B_x - \beta_x B_z) \tag{22}$$

that is, by virtue of (8)

$$\frac{d\beta_y}{dz} \approx \frac{e}{\gamma m c} \left(B_x - \frac{\beta_x}{\beta_z} B_z \right) = \frac{e}{\gamma m c} \left(B_x - \frac{dx}{dz} B_z \right) \tag{23}$$

i.e.

$$\frac{d^2 y}{dz^2} \approx \frac{e}{\gamma \beta_z m c} \left(B_x - \frac{dx}{dz} B_z \right) \tag{24}$$

Since the reference trajectory is merely $y = y' = 0$, eq. (24) defines directly the ‘‘error’’ equation:

$$y_\delta \approx y \tag{25}$$

Substitution of field’s components from eq. (5) yields

$$\frac{d^2 y_\delta}{dz^2} \approx \frac{e B_0 k_u}{\gamma \beta_z m c} \left[-\delta \frac{k_u}{2} x(z) \sin(k_u z) - \frac{dx}{dz} \cos(k_u z) \right] y_\delta(z) \tag{26}$$

In previous result one can put safely $x(z) \equiv x_r(z)$ and $\frac{dx}{dz} \equiv \frac{dx_r}{dz}$. Insertion of (17) and its derivative

$$\frac{dx_r}{dz} = -\frac{K}{\gamma} \cos(k_u z)$$

yields

$$\begin{aligned}
\frac{d^2 y_\delta}{dz^2} &\approx \frac{e B_0 k_u}{\gamma \beta_z m c} \left[\frac{\delta K}{2 \gamma} \sin^2(k_u z) + \frac{K}{\gamma} \cos^2(k_u z) \right] y_\delta(z) \\
&= \frac{1}{2} \frac{e B_0 k_u}{\gamma^2 \beta_z m c} K \left[\delta \sin^2(k_u z) + 2 \cos^2(k_u z) \right] y_\delta(z) \\
&= -\frac{k_u^2 K^2}{2 \gamma^2 \beta_z} \left[\delta \sin^2(k_u z) + 2 \cos^2(k_u z) \right] y_\delta(z)
\end{aligned} \tag{27}$$

Average on an undulator period (λ_u) gives the result

$$\begin{aligned} \left\langle \frac{d^2 y_\delta}{dz^2} \right\rangle &\approx -\frac{k_u^2 K^2}{4\gamma^2 \beta_z} [2 + \delta] y_\delta(z) \\ &= -\frac{1}{\beta_z} \left(\frac{\pi K}{\gamma \lambda_u} \right)^2 [2 + \delta] y_\delta(z) \end{aligned}$$

which can be approximated (for $\beta_z \approx 1$) to

$$\boxed{\left\langle \frac{d^2 y_\delta}{dz^2} \right\rangle \approx -[2 + \delta] \left(\frac{\pi K}{\gamma \lambda_u} \right)^2 y_\delta(z)} \quad (28)$$

Eqs. (21) and (28) state that transverse motion is subject to a linear defocusing (x) or focusing (y) force, with a much stronger coupling in vertical than horizontal direction. It should be stressed that this analysis refers to “errors” with respect to reference orbit. On a global respect, motion can be described - quite expectedly - as a sequence of alternate dipoles. The linear maps describing the effect of the undulator are

$$\begin{aligned} \begin{pmatrix} x \\ x' \end{pmatrix} &= \begin{pmatrix} \cosh \sqrt{\kappa_x} z & \frac{\sinh \sqrt{\kappa_x} z}{\sqrt{\kappa_x}} \\ \sqrt{\kappa_x} \sinh \sqrt{\kappa_x} z & \cosh \sqrt{\kappa_x} z \end{pmatrix} \begin{pmatrix} x_0 \\ x'_0 \end{pmatrix} & \kappa_x &= \delta \left(\frac{\pi K}{\gamma \lambda_u} \right)^2 \\ \begin{pmatrix} y \\ y' \end{pmatrix} &= \begin{pmatrix} \cos \sqrt{\kappa_y} z & \frac{\sin \sqrt{\kappa_y} z}{\sqrt{\kappa_y}} \\ -\sqrt{\kappa_y} \sin \sqrt{\kappa_y} z & \cos \sqrt{\kappa_y} z \end{pmatrix} \begin{pmatrix} y_0 \\ y'_0 \end{pmatrix} & \kappa_y &= (2 + \delta) \left(\frac{\pi K}{\gamma \lambda_u} \right)^2 \approx 2 \left(\frac{\pi K}{\gamma \lambda_u} \right)^2 \end{aligned} \quad (29)$$

III. MATCHING CONDITIONS IN THE SPARC UNDULATOR.

The layout of SPARC experiment, downward the three TW accelerating sections, is shown in fig. (2). In tables (I) and (II)[5] are resumed the positions, sizes and main features of the relevant devices. The coefficients c_1 e c_2 are the results of a fit to the following parametrization of undulator’s strength[6]:

$$K(g) = c_1 \cdot \exp(-c_2 \cdot g) \quad (30)$$

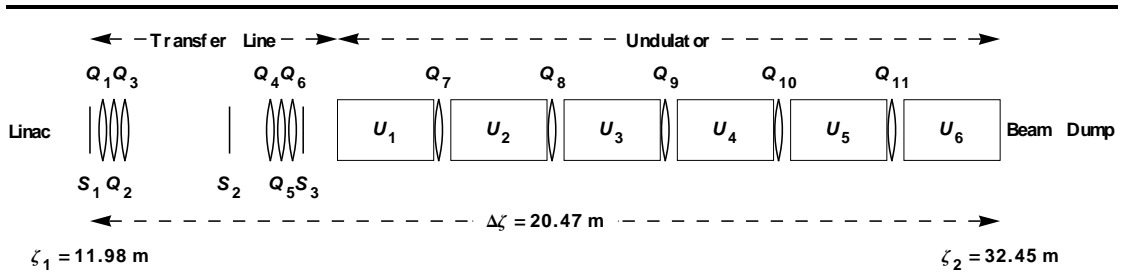


Figure 2

Layout of SPARC transfer line (quads $Q_1 \rightarrow Q_6$) and undulator (quads $Q_7 \rightarrow Q_{11}$ + undulator sections $U_1 \rightarrow U_6$) of SPARC experiment. The S 's tag the positions of imaging screens, the ζ 's measure the distance from photo-cathode.

	Q_1	Q_2	Q_3	Q_4	Q_5	Q_6	Q_7	Q_8	Q_9	Q_{10}	Q_{11}
ζ [m]	12.267	12.518	12.765	16.036	16.286	16.5362	19.824	22.372	24.919	27.468	30.016
L_{eff} [mm]	171.700	172.600	172.600	172.000	169.900	171.700	53.260	54.440	52.590	54.600	53.660
τ [$\frac{\text{T}}{\text{A}\cdot\text{m}}$]	0.7863	0.7880	0.7880	0.8095	0.7864	0.8055	3.100	3.043	3.038	3.158	3.058

Table I

Quadrupole synoptics (Transfer Line+Undulator). The L_{eff} tag the effective lengths, τ 's the strength calibration constants.

	U_1	U_2	U_3	U_4	U_5	U_6
ζ [m]	18.629	21.178	23.725	26.273	28.821	31.370
L [mm]	2164.14	2163.76	2164.06	2164.51	2164.57	2164.31
c_1	5.735	5.708	5.716	5.88	5.671	5.751
c_2 [mm^{-1}]	0.1131	0.1126	0.1121	0.113	0.1122	0.1122

Table II

Undulator synoptics. Positions (ζ) measure the distance from cathode. See formula (30) for the meaning of coefficients c_1 and c_2

For accelerators, the expression "beam matching" refers to the adjustment of beam optics to the device lattice to meet the requirements necessary for operation. The concrete implementation of this concept may differ substantially depending on the general properties of the accelerator and the experimental goals. In circular machines, usually this means imposing periodic conditions over the entire length of the accelerator or a sub-multiple of it. In the magnetic undulator of a single passage FEL[7, 8], on the other hand, "matching the beam" means optimizing the coupling between electron beam and radiation. In the case of several undulator sections alternated with quadrupoles and all tuned to the same wavelength, one may well want to impose periodical conditions over the distance spanned by the single undulator+quadrupole unit (which includes any drift between the two devices or up to the leading edge of next undulator section). This means essentially realizing at the leading edge of the unit an eigenstate of the corresponding Twiss transport matrix associated to the eigenvalue $\lambda = 1$. All the other sections will be "matched" accordingly. Notwithstanding, a number of reasons may render impossible or useless this approach:

- the undulator sections are set to resonate at different wavelengths, as in a "cascade" FEL[9] experiment; this means that - each undulator being set as to feature different optical properties - may well turn to be impossible - and there is no use in - transporting the beam so that at lattice boundary it presents itself as an eigenstate of the following unit;
- the (3×3) Twiss matrix corresponding to a physical device always invariably admits the real eigenvalue $\lambda = 1$ (see (37) below). The corresponding $((\beta_x, \alpha_x, \gamma_x)$ and $(\beta_y, \alpha_y, \gamma_y))$ eigenstates (up to multiplicative constants) are obviously the ones of choice if the beam is to be transported through a lattice of identical undulator sections. In the case of SPARC lattice, this means that, given the focusing properties of the undulator (uniquely defined by the beam energy and gap), such states exist whatever the current of the following quadrupole. It must be noted, however, that they do not necessarily describe physical beams (see below). Moreover, since a (plane) magnetic undulator has different optical properties in vertical and horizontal directions (as shown in section (II)), it may turn

to be impossible - once the resonant wavelength $\lambda_r(g, \gamma)$ has been set - to arrange the quadrupole to obtain eigenstates of the Twiss transport matrix describing *physical beams* in *both* vertical and horizontal directions.

In what follows the above points will be analyzed in some detail, with a general digression and some examples of real experimental situations.

In the framework of linear beam dynamics[10, 11], the motion of a particle in the phase-space is described in matrix formulation by

$$\begin{pmatrix} u(z) \\ u'(z) \end{pmatrix} = \begin{pmatrix} C_u(z) & S_u(z) \\ C'_u(z) & S'_u(z) \end{pmatrix} \begin{pmatrix} u_0 \\ u'_0 \end{pmatrix} \quad u = x, y$$

The matrix

$$\mathcal{M}_u(z) = \begin{pmatrix} C_u(z) & S_u(z) \\ C'_u(z) & S'_u(z) \end{pmatrix} \quad (31)$$

permits a detailed ray-tracing of any given particle through the accelerator. It is the product of the matrices composing the sequence of devices:

$$\mathcal{M}_u = \mathcal{M}_u^{(n)} \dots \mathcal{M}_u^{(2)} \cdot \mathcal{M}_u^{(1)}$$

Since for each device the condition

$$\det \mathcal{M}_u^{(i)} = 1 \quad (32)$$

is fulfilled (a general properties of evolution operators in linear Hamiltonian dynamics) , it is easily seen that the same applies to the whole matrix \mathcal{M}_u in (31).

Liouville's theorem for the beam particle phase-space density distribution $\rho(\mathcal{U})$

$$\frac{d\rho(\mathcal{U})}{dz} = 0 \quad \text{where} \quad \mathcal{U} \equiv \begin{pmatrix} u \\ u' \end{pmatrix}$$

implies that

$$\rho(\mathcal{U}) = \rho(\mathcal{M}\mathcal{U}^0) = \rho(\mathcal{U}^0)$$

The r.m.s. matrix:

$$\widehat{\Sigma} \equiv \int \mathcal{U} \rho(\mathcal{U}) \mathcal{U}^T d\mathcal{U}$$

evolves in time according to the following expression:

$$\begin{aligned} \widehat{\Sigma}_u(z) &= \int [\mathcal{M}_u(z) \mathcal{U}^0] \rho(\mathcal{M}_u(z) \mathcal{U}^0) [\mathcal{M}_u(z) \mathcal{U}^0]^T d[\mathcal{M}_u(z) \mathcal{U}^0] \\ &= \mathcal{M}_u(z) \left\{ \int \mathcal{U}^0 \rho(\mathcal{U}^0) \mathcal{U}^{0T} \left[\overbrace{\det \mathcal{M}_u^T(z)}^{=1} d\mathcal{U}^0 \right] \right\} \mathcal{M}_u^T(z) \\ &= \mathcal{M}_u(z) \widehat{\Sigma}^0 \mathcal{M}_u^T(z) \end{aligned} \quad (33)$$

Normalized emittance ϵ is defined as $\epsilon = \sqrt{\det \widehat{\Sigma}}$ (note that $\det \widehat{\Sigma} > 0$ since $\widehat{\Sigma}$ is a real, symmetric, non singular matrix). A consequence of (32) and (33) is that emittance is a conserved quantity. The r.m.s. matrix can put then in the form

$$\widehat{\Sigma}_u = \epsilon_u \begin{pmatrix} \beta_u & \alpha_u \\ \alpha_u & \gamma_u \end{pmatrix} \quad (34)$$

where the Twiss coefficients β_u, α_u and γ_u are thus constrained by the condition

$$\mathcal{N}(\beta_u, \alpha_u, \gamma_u) \equiv \beta_u \gamma_u - \alpha_u^2 = 1 \quad (35)$$

A consequence of (34) is that $\epsilon_u \beta_u$ and $\epsilon_u \gamma_u$ represent the variance of u and u' , respectively - two strictly positive quantities - so β_u and γ_u must be strictly positive as well. Quantity $\epsilon \alpha_u$ expresses instead the correlation between u and u' in the phase-space. It is easily shown that evolution of Twiss coefficients is governed by the following expression:

$$\begin{pmatrix} \beta_u \\ \alpha_u \\ \gamma_u \end{pmatrix} = T(\mathcal{M}_u) \begin{pmatrix} \beta_u^0 \\ \alpha_u^0 \\ \gamma_u^0 \end{pmatrix}$$

where

$$T(\mathcal{M}_u) = \begin{pmatrix} C_u^2 & -2C_u S_u & S_u^2 \\ -C_u C'_u & S_u C'_u + C_u S'_u & -S_u S'_u \\ C_u'^2 & -2C'_u S'_u & S_u'^2 \end{pmatrix} \quad (36)$$

Moreover, it can be shown that the eigenvalues of (36) are

$$\lambda_1 = C_u S'_u - S_u C'_u = \det \mathcal{M}_u = 1 \quad (37)$$

$$\lambda_{2/3} = \frac{1}{2} \left[\left(C_u^2 + 2S_u C'_u + S_u'^2 \mp (C_u + S'_u) \sqrt{(C_u - S'_u)^2 + 4S_u C'_u} \right) \right]$$

The eigenvector associated to $\lambda_1 = 1$ is obviously the only candidate whenever one wants to leave optical functions β, α, γ unchanged at the exit of a device. The eigenvector corresponding to unit eigenvalue is

$$v^{(1)} = \begin{pmatrix} 2S_u \\ C_u - S'_u \\ -2C'_u \end{pmatrix}$$

up to a real multiplicative constant r to be found to enforce condition (35). One can set this multiplicative constant to

$$r \equiv \frac{v_1}{|v_1|} \frac{1}{\sqrt{|v_1 v_3 - v_2^2|}} \quad (38)$$

where $v^{(1)} = (v_1, v_2, v_3)$ is the eigenvector associated to $\lambda_1 = 1$ and

$$\tilde{v} \equiv \begin{pmatrix} \beta_u \\ \alpha_u \\ \gamma_u \end{pmatrix} = r v = \begin{pmatrix} r v_1 \\ r v_2 \\ r v_3 \end{pmatrix}$$

the rescaled eigenvector. The choice (38) has the merit to force β_u to the positive value

$$\beta_u = \frac{v_1^2}{|v_1|} \frac{1}{\sqrt{|\mathcal{N}(v)|}} = \frac{|v_1|}{\sqrt{|\mathcal{N}(v)|}}$$

Note, however, that

$$\mathcal{N}(\tilde{v}) \equiv \beta_u \gamma_u - \alpha_u^2 = r^2 \mathcal{N}(v) = \frac{\mathcal{N}(v)}{|\mathcal{N}(v)|} = \pm 1 \quad (39)$$

The last result deserves a few comments: there is no warranty that the eigenvector associated to the eigenvalue $\lambda_1 = 1$ fulfills the Twiss condition (35). Consider the case, for example, that

$$v_1 v_3 \leq 0$$

or (more generally)

$$\mathcal{N}(v) = v_1 v_3 - v_2^2 \leq 0$$

Since rescaling of the eigenvector by any constant r amounts to multiply $v_1 v_3$ or $v_1 v_3 - v_2^2$ by r^2 , there is no chance to make β_u and γ_u to represent *both* strictly positive quantities (the product $\beta_u \gamma_u = r^2 v_1 v_3 \leq 0$ remains negative), or $\beta_u \gamma_u - \alpha_u^2 = r^2 (\beta_u \gamma_u - \alpha_u^2)$ to become positive. These conditions (i.e. $\mathcal{N}(v) \leq 0$) signal that *matching is impossible*, that is an eigenvector associated to eigenvalue $\lambda_1 = 1$ exists, but it *cannot* be re-scaled to represent any *physical* beam. An apodictic - and limit - case is that of drift, for which the Twiss matrix reads

$$\mathcal{D}_u(L) = \begin{pmatrix} 1 & -2L & L^2 \\ 0 & 1 & -L \\ 0 & 0 & 1 \end{pmatrix}$$

with characteristic polynomial $P(\lambda) = (1 - \lambda)^3$ and eigenvector

$$v = \begin{pmatrix} 1 \\ 0 \\ 0 \end{pmatrix}$$

In this case the Twiss form $\mathcal{N}(v)$ is identically zero. Trivial considerations confirm that the only eigenstate is obviously that of a beam with no slope dispersion ($\gamma_u = 0$).

For undulators, *matching* conditions must be fulfilled simultaneously in vertical and horizontal directions, which aggravates the problem since the focusing/defocusing properties of the quadrupole following the undulator section are determined by one and the same current value, and it may well happen that for any given current permissible in the range of the device, the condition discussed above (the eigenstate exists, but it is unphysical) applies to one of the two directions, or both. Consider, in this regard, a lattice unit composed (as for SPARC experiment) by an undulator section, a drift, a quadrupole and another drift up to the leading edge of the following section. A rough estimation of the current limits for which physical eigenstates for such a device exist, can be found assuming that the undulator behaves in the horizontal direction as a drift. It can be shown - quite expectedly - that no physical eigenstates may exist if the quadrupole is defocusing horizontally. If the convention that the quadrupole is focusing vertically for positive currents, this means that physical horizontal eigenstates may exist only for $I_Q < 0$. In this case it can be shown that the (un-normalized) horizontal eigenstate reads

$$v_x = \left\{ \frac{(L_{D_1} + L_{D_2} + L_U) \cot(L_Q \sqrt{\kappa_Q})}{\sqrt{\kappa_Q}} - (L_{D_1} + L_U) L_{D_2} + \frac{1}{\kappa_Q}, \frac{1}{2} (L_{D_1} - L_{D_2} + L_U), 1 \right\} \quad (40)$$

The form $(\beta_x \gamma_x - \alpha_x^2)$ in this case reads

$$\mathcal{N}_x(v) = \frac{(L_{D_1} + L_{D_2} + L_U) \cot(L_Q \sqrt{\kappa_Q})}{\sqrt{\kappa_Q}} + \frac{1}{\kappa_Q} - \frac{1}{4} (L_{D_1} + L_{D_2} + L_U)^2 \quad (41)$$

The Twiss condition (35) can be realized provided expression (41) is positive. If the condition $L_Q \sqrt{\kappa_Q} \ll 1$ holds, then $\cot(L_Q \sqrt{\kappa_Q}) \approx 1/(L_Q \sqrt{\kappa_Q})$ and (41) collapses to:

$$\mathcal{N}_x(v) = \frac{L_{D_2} + L_{D_1} + L_U + L_Q}{L_Q \kappa_Q} - \frac{1}{4} (L_{D_2} + L_{D_1} + L_U)^2 \quad (42)$$

and

$$\mathcal{N}_x(v) \geq 0 \iff \kappa_Q L_Q \leq 4 \frac{L_{D_2} + L_Q + L_{D_1} + L_U}{(L_{D_1} + L_{D_2} + L_U)^2} \quad (43)$$

Since

$$\kappa_Q L_Q = \frac{1}{|f|} = \frac{e}{\gamma m c} \eta \cdot |I_Q| = \frac{0.3 \eta [\text{T/A}]}{E [\text{GeV}]} |I_Q [A]|$$

(η is the calibration constant yielding the integrated gradient per unit current) (43) reduces to

$$\left| I_Q [A] \right| < 4 \frac{E [\text{GeV}]}{0.3\eta [\text{T/A}]} \frac{L_U + L_{D_1} + L_Q + L_{D_2}}{(L_{D_1} + L_{D_2} + L_U)^2} \quad (44)$$

that is

$$\boxed{-4 \frac{E [\text{GeV}]}{0.3\eta [\text{T/A}]} \frac{L_U + L_{D_1} + L_Q + L_{D_2}}{(L_{D_1} + L_{D_2} + L_U)^2} < I_Q [A] < 0} \quad (45)$$

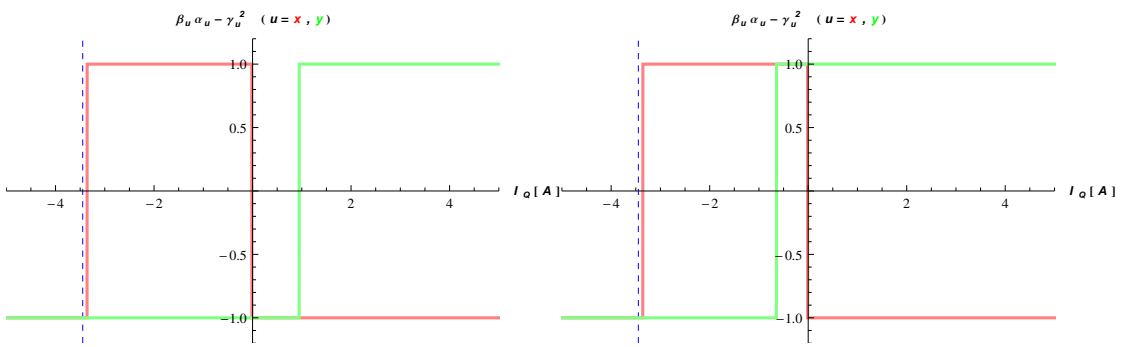


Figure 3

Twiss “norm” (eq. (35)) for lattice eigenstates in horizontal (red) and vertical (green) directions for 1st undulator section, for a beam with $\gamma = 205$ ($E = 105\text{MeV}$) set at gaps: $g = 10.88$ (left) ($K = 1.675$, $\lambda_r = 800\text{nm}$) and $g = 11.275\text{mm}$ (right) ($K = 1.602$, $\lambda_r = 760\text{nm}$), as a function of the current in the downward quad. A positive current means that the quadrupole is focusing vertically and defocusing horizontally. Matching is possible within the current interval where $\beta\gamma - \alpha^2 = 1$ in both x and y directions. No such interval exists in the first case. In the later the situation is reversed.

The value corresponding to (45) is signaled in figs. (3) by the dashed vertical line. Since the value is very close to that corresponding to the transition from unphysical to physical eigenstates, the approximation used seems fairly good.

The case for the vertical direction is far more complicated and eludes any attempt of exact analytical treatment. Therefore, the existence of a physical vertical eigenstate compatible with (45) (that is, consistent with the condition that $I_Q \leq 0$) must be studied numerically. In fig. (4) the eigenstate’s maximum Twiss norm (as a function of the quadrupole current) is displayed as a function of the gap (left plot) for the same beam parameters as in fig. (3). To get rid of energy dependence, yet at the price of more abstraction, it is useful to cast the same result in terms of $\kappa_{U,y}$ alone (right plot). What matters really in fig. (4) is the sign of \mathcal{N}_{\max} . From the plot of \mathcal{N}_{\max} vs g is clear, for example, that no physical vertical eigenstate exist for $9.83\text{mm} \lesssim g \lesssim 11.21\text{mm}$. The plot of \mathcal{N}_{\max} vs $\kappa_{U,y}$, on the other hand, is more universal, since it applies to any combination of parameter values conspiring to build up the same value of $\kappa_{U,y}$. The previous constraint, in fact, translates to

$$\begin{aligned} \kappa_{U,y}^{(1)} &\leq (2 + \delta) \left(\frac{\pi K}{\gamma \lambda_U} \right)^2 \leq \kappa_{U,y}^{(2)} \\ \kappa_{U,y}^{(3)} &\leq (2 + \delta) \left(\frac{\pi K}{\gamma \lambda_U} \right)^2 \leq \kappa_{U,y}^{(4)} \\ \kappa_{U,y}^{(5)} &\leq (2 + \delta) \left(\frac{\pi K}{\gamma \lambda_U} \right)^2 \leq \kappa_{U,y}^{(6)} \end{aligned} \quad (46)$$

...

where $\kappa_{U,y}^{(1)} \approx 1.53$, $\kappa_{U,y}^{(2)} \approx 2.11$, $\kappa_{U,y}^{(3)} \approx 6.23$, $\kappa_{U,y}^{(4)} \approx 8.43$, $\kappa_{U,y}^{(5)} \approx 14.33$ and $\kappa_{U,y}^{(6)} \approx 18.97$.

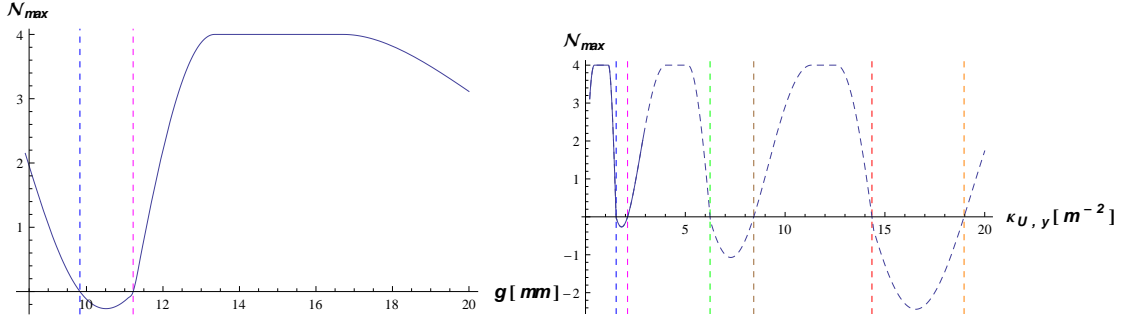


Figure 4

Maximum of Twiss “norm” (eq. (35)) for lattice eigenstates in vertical direction for 1st undulator section as a function of the gap (left) and $\kappa_{U,y}$ (right, solid). The maximum is found by varying the quadrupole current in the range $-10\text{A} \leq I_Q \leq 0$. Beam parameters are the same as in fig. (3). Dashed vertical lines delimit the region where no physical matching is possible.

In the right plot of fig. (4) the solid line refers to a beam of $\gamma \approx 206$, with the undulator gap spanning the interval $8.4 \div 20\text{cm}$. The same curve, including the dashed line, on the other hand, refers to the same gap interval for a beam of energy decreased by a factor 2.5 ($\gamma \approx 82$). The (46) can be reduced to a more suggestive form by casting the undulator strength parameter K in terms of the resonant wavelength λ_r and the beam energy γ , which yields

$$\kappa_{U,y} = 4\pi^2 \frac{2\gamma^2 \lambda_r - \lambda_U}{\gamma^2 \lambda_U^3} \quad (47)$$

Equation (47) can be used express the resonant wavelength *vs* beam energy corresponding to a given value κ_U . The curves in fig. (5) plot λ_r as a function of beam energy for $\kappa_{U,y} = \kappa_{U,y}^{(i)}$ where $\kappa_{U,y}^{(i)}$ are the zeros of \mathcal{N}_{\max} . The shaded regions delimit the band-like *forbidden* zones where no physical vertical eigenstates can be realized with a single defocusing quadrupole.

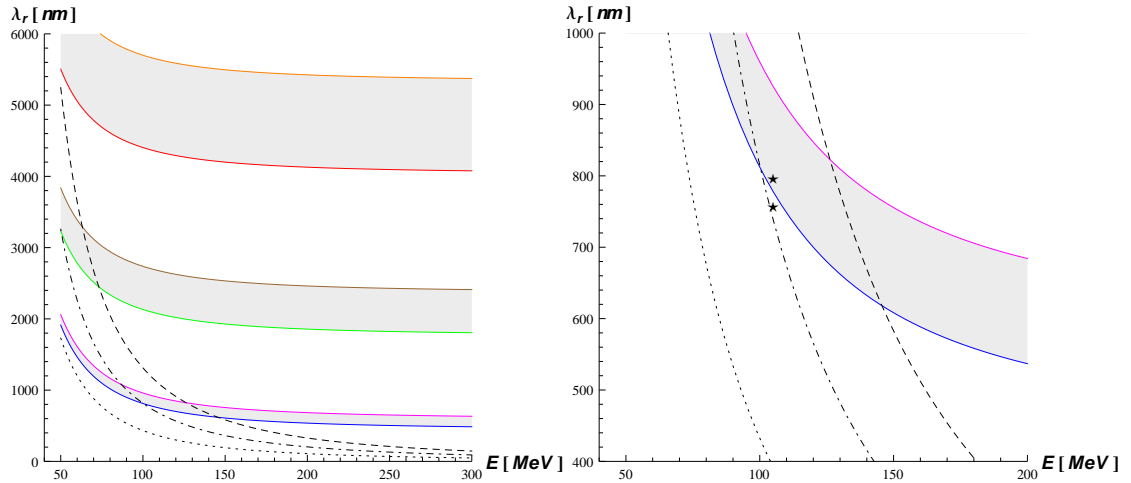


Figure 5

Left: resonant wavelength *vs* beam energy (eq. (47)) corresponding to $\kappa_U = 1.53, 2.11, 6.23 \dots$ (see text). In the shaded regions it is impossible to realize physical vertical eigenstates with a single defocusing quadrupole. The black lines correspond to curves where the gap has been kept fixed to $g = 8.2\text{mm}$ (dashed), $g = 11.5\text{mm}$ (dash-dotted) and $g = 20\text{mm}$ (dotted), respectively. Right: the same as in left plot, zoomed to a region relevant for SPARC operation. The asterisks refer to the cases described in fig. (3).

IV. OPTIMIZATION. TRANSFER LINE QUADS.

Optimization of FEL performances can be achieved by identifying the value of quadrupole current downward the undulator which correspond to an extreme (usually a minimum) of a suitably defined merit functional. Some possible choices are:

$$\chi^2 = \int_{LU} \beta_x \cdot \beta_y d\zeta \quad (48)$$

$$\chi^2 = \int_{LU} (\epsilon_x \beta_x - \epsilon_y \beta_y)^2 d\zeta \quad (49)$$

$$\chi^2 = \int_{LU} (\epsilon_x \beta_x + \epsilon_y \beta_y) d\zeta \quad (50)$$

$$\chi^2 = \int_{LU} (\epsilon_x \beta_x + \epsilon_y \beta_y) (\epsilon_x \beta_x - \epsilon_y \beta_y)^2 d\zeta \quad (51)$$

...

The dependence of functionals (48-51) on the quadrupole current are plotted in fig. (6) (top graphs) for two working points chosen in two different *allowed* regions. The crosses tagging the minima identify the eigenvectors optimizing the beam parameters. Functional (48) and (50), for example, are designed to minimize the average cross section of the electron beam, functional (49) is designed to obtain a *round* beam, and functional (51) is a compromise between size and roundness.

Once the optimal x, y eigenstates for the undulator section have been found along with the associated current to be fed to the downward quadrupole, one is left with the final problem of finding the settings for the quadrupole of the transfer line that realize these states given the beam properties at the end of acceleration stage. The mathematical problem to be solved is a set of 2×3 nonlinear equations for the currents of an equal number of transfer line quadrupole:

$$\begin{pmatrix} \beta_u^{(1)} \\ \alpha_u^{(1)} \\ \gamma_u^{(1)} \end{pmatrix} = T(\mathcal{M}_{u,TL}) \begin{pmatrix} \beta_u^{(0)} \\ \alpha_u^{(0)} \\ \gamma_u^{(0)} \end{pmatrix} \quad u = x, y$$

where $\mathcal{M}_{u,TL}(\{I_{TL}\})$ is the transport matrix from the end of acceleration stage up to the entrance of undulator section, which depends of course on the (equal number of) currents $\{I_{TL}\}$ of transfer line quadrupoles. Note that since β_u, α_u and γ_u ($u=x,y$) are not independent for Twiss condition (35) is naturally preserved, in principle the number of unknowns may be reduced by two (from 6 to 4). Nevertheless, it must be remarked that the problem at hand is non-linear, so there is no guarantee that a solution exists. Playing around with a numerical code implemented specifically to handle both cases, clearly shows that solving the complete (6 equations in 6 unknowns), covertly over-determined problem, turns to be a more robust choice (capability of finding a solution). In fig. (7) are shown a few examples of matching obtained with different gap values. In the third case (beam energy and resonant wavelength purposely chosen to be very close to the “forbidden zone” where no physical eigenstates exist in the undulator lattice) no matching could be found with only 4 independent quadrupoles.

V. CONCLUSIONS

In this note the focusing properties of SPARC undulators have been discussed, along with the analytical conditions to be fulfilled for transporting the beam through the periodic lattice of undulator’s sections. It has been shown that band-like *forbidden* zones can be identified in the plane (E_b, λ_r) of resonant wavelengths vs electron beam energy, where no physical eigenstates can be realized simultaneously in both transverse directions, in the considered elementary lattice unit. A proper choice of beam energy and undulator gap in an allowed region of the diagram in Fig. 5, allows steadily operation of undulators mainly designed to function in the lowermost region of the plane (λ_r, E_b) at considerably larger wavelengths.

Acknowledgments

We warmly acknowledge B. Di Viacco for useful discussions and encouragement.

-
- [1] O. Chubar P. Elleaume and J. Chavanne. Computing 3d magnetic fields from insertion device. *PAC97 Conference*, 1997.
 - [2] P. Elleaume O. Chubar and J. Chavanne. A 3d magnetostatics computer code for insertion devices. *SRI97 Conference*, 1997.
 - [3] Radia homepage <http://www.esrf.eu/accelerators/groups/insertiondevices/software/radia>.
 - [4] F. Ciocci, G. Dattoli, A. Torre, and A. Renieri. *Insertion Devices for Synchrotron Radiation and Free Electron Laser - Series on Synchrotron Radiation Techniques and Applications*, volume 6. World Sci. Books, 2000.
 - [5] C. Ronsivalle. private communication.
 - [6] M. Quattromini et al. Detailed k and phase error analysis of the sparcs undulator. Technical report, SPARC, 2009/005.
 - [7] H. Haus. Noise in free-electron laser amplifier. *Quantum Electronics, IEEE Journal of*, 17(8):1427 – 1435, aug. 1981.
 - [8] R. Bonifacio, C. Pellegrini, and L. M. Narducci. Collective instabilities and high-gain regime in a free-electron laser. *Opt. Comm.*, 50:373, 1984.
 - [9] L. Giannessi and P. Musumeci. The free-electron laser harmonic cascade. *New Journal of Physics*, 8(11):294, 2006.
 - [10] H. Wiedemann. *Particle Accelerator Physics*. Springer, 3rd edition, 2007.
 - [11] E.D. Courant and H.S. Snyder. Theory of the alternating-gradient synchrotron. *Annals of Physics*, 281:360–408, 1958.

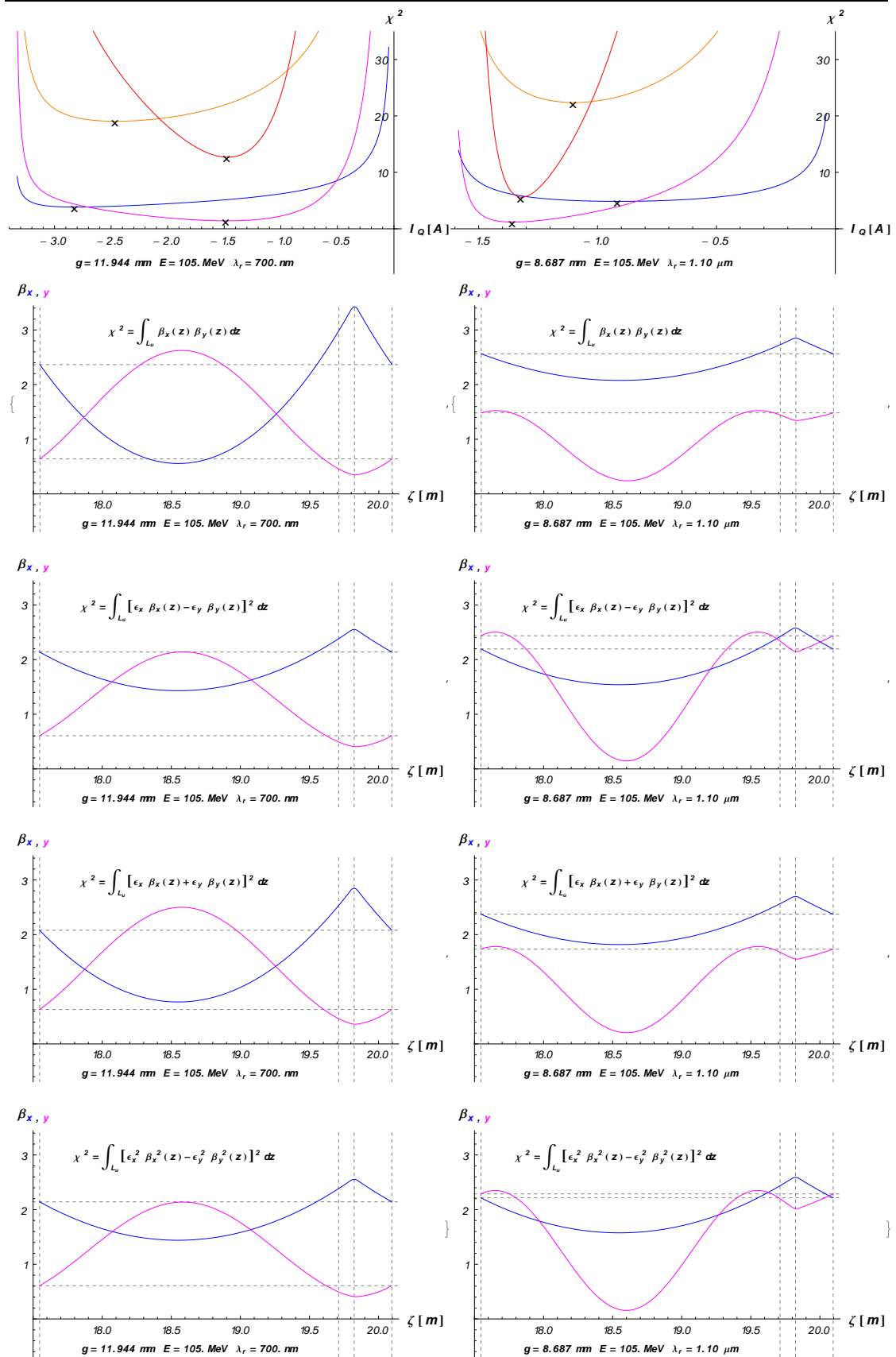


Figure 6

Top: merit functionals for undulator eigenstates corresponding to the quadrupole current (in abscissa) for a beam energy of 105 MeV ($\gamma \approx 205$) and gap values (left) $g = 11.944$ nm ($\lambda_r = 700$ nm) and (right) $g = 8.687$ nm ($\lambda_r = 1.1 \mu\text{m}$). Blue, magenta, orange and red curves correspond to functionals (48), (49), (50), and (51), respectively; 2nd \rightarrow 5th row: optical functions β_x (blue) and β_y (magenta) for eigenstates corresponding to the χ^2 minima (the crosses in the top plots).

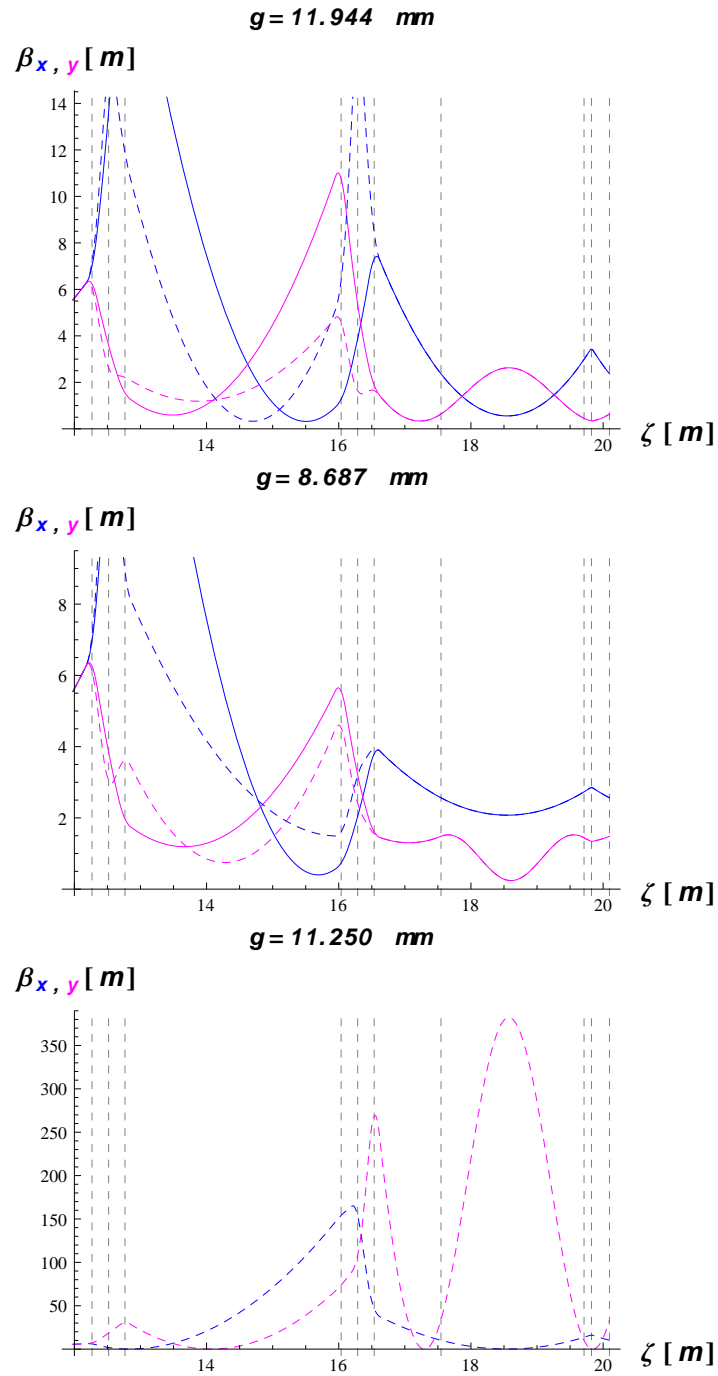


Figure 7

Matching from the transfer line up to the first undulator section for three different gaps. Solid and dashed lines refer to the solution obtained with 4 and 6 transfer line independent quadrupoles, respectively. The eigenstates in the undulator correspond to optimum found by minimizing functional (48). For the third gap (11.250mm) only the matching with 6 quads is shown, for it proved problematic to find a solution with 4. The vertical dashed lines tag the positions of TL- quads, and those shown in fig. (6). The beam energy is 105MeV in all cases.